

Optimal extended homotopy analysis method for Multi-Degree-of-Freedom nonlinear dynamical systems and its application

Y.H. Qian* and Y.F. Zhang

College of Mathematics, Physics and Information Engineering, Zhejiang Normal University, Jinhua, Zhejiang 321004, P.R. China

(Received May 4, 2016, Revised July 27, 2016, Accepted September 27, 2016)

Abstract. In this paper, the optimal extended homotopy analysis method (OEHAM) is introduced to deal with the damped Duffing resonator driven by a van der Pol oscillator, which can be described as a complex Multi-Degree-of-Freedom (MDOF) nonlinear coupling system. Ecumenically, the exact solutions of the MDOF nonlinear coupling systems are difficult to be obtained, thus the development of analytical approximation becomes an effective and meaningful approach to analyze these systems. Compared with traditional perturbation methods, HAM is more valid and available, and has been widely used for nonlinear problems in recent years. Hence, the method will be chosen to study the system in this article. In order to acquire more suitable solutions, we put forward HAM to the OEHAM. For the sake of verifying the accuracy of the above method, a series of comparisons are introduced between the results received by the OEHAM and the numerical integration method. The results in this article demonstrate that the OEHAM is an effective and robust technique for MDOF nonlinear coupling systems. Besides, the presented methods can also be broadly used for various strongly nonlinear MDOF dynamical systems.

Keywords: optimal extended homotopy analysis method; Duffing resonator; van der Pol oscillator; coupling stiffness; Multi-Degree-of-Freedom

1. Introduction

Due to the actual needs in mechanical aspects, an increasing number of researchers have been dedicated to developing some behaviors of complex dynamical systems, such as periodic solutions, stability analysis and bifurcation analysis. But it is an arduous task to receive exact solutions of the above systems. We can consider some simple cases as a foundation, from which we may get some useful inspiration. Thus, in this paper, we will consider such a nonlinear system as follows

$$\begin{cases} \ddot{x}_1 + \varepsilon_1 \dot{x}_1 + \Omega_1^2 x_1 + k_1 x_1^3 - k_c(x_2 - x_1) = 0 \\ \ddot{x}_2 + \varepsilon_2(x_2^2 - 1)\dot{x}_2 + \Omega_2^2 x_2 - k_c(x_1 - x_2) = 0 \end{cases} \quad (1)$$

where x_1 , ε_1 , Ω_1 and x_2 , ε_2 , Ω_2 are the displacement, damping coefficient and linear frequency of the van der Pol oscillator respectively. Moreover, k_1 is nonlinear stiffness of the Duffing resonator, and k_c is coupled linear stiffness between the two resonators. If k_c is equal to zero, Eq. (1) is an uncoupled system.

For this type of periodical system, the dynamics have been explored in the circumstance of 1:1 internal resonance and different coupling stiffness in the past few years by Wei, Randrianandrasana *et al.* (2011). Also, the angular frequency and steady state amplitude of the governing equation in this paper have been investigated by residue harmonic balance methods. But it is an almost impossible

task to gain the exact solutions. Therefore, a variety of methods are presented to obtain its analytical approximate solutions, such as matrix perturbation method by Lu, Feng *et al.* (1991), modified decomposition method by Ray *et al.* (2006), complex variable functions method by Lu, Feng *et al.* (2012), harmonic balance methods by Guo, Leung *et al.* (2011), residue harmonic balance methods by Leung and Guo (2010). The free vibration analysis of axially moving beams is investigated according to Reddy-Bickford beam theory (RBT) by using dynamic stiffness method (DSM) and differential transform method (DTM) by Bozyigit and Yesilce (2016). However, on account of the complexity of the process and operation, the analytical approximation solutions are difficult to be explored.

Liao (1992) put forward a general analytical technique for such a nonlinear problem, named homotopy analysis method (HAM), which is based on a notion of the homotopy in topology. Different from other perturbation methods, it does not depend on small parameter. Moreover, it provides a valid approach to control the convergence of series solutions. In the past two decades, a lot of attention has been paid to using the HAM to solve engineering and physics problems. Qian and Chen (2010) developed the multi-degree-of-freedom (MDOF) coupled van der Pol Duffing oscillators by HAM. Vishal, Kumar *et al.* (2011) used the HAM to deal with fractional Swift Hohenberg equation-Revisited. Tasbozan, Esen *et al.* (2015) gained approximate analytical solution of fractional coupled mKdV equation by HAM. Hoshyar, Ganji *et al.* (2015) explored the analytical solutions of the flow of incompressible Newtonian fluid between two parallel plates by HAM. Handam, Freihat *et al.* (2015) studied the approximate analytical solutions of the HIV infection model of CD4+T

*Corresponding author,
E-mail: qyh2004@zjnu.edu.cn

cells of fractional order by multi-step HAM.

Along with the actual needs, the HAM was developed by some pathfinders. Zhang, Qian *et al.* (2012) utilized the extended homotopy analysis method (EHAM) to obtain the periodic solutions of MDOF strongly nonlinear coupled van der Pol-Duffing oscillators, successfully. Further more, the modified HAM by Xin, Kumar *et al.* (2015) is introduced to get the analytical solutions of wave-like fractional physical models. It can obtain perfect results by using Laplace transform and HAM. Hence, we can conclude that the EHAM is valid and acceptable. In particularly, the approach is suitable for solving MDOF strongly nonlinear problems. Certainly, the method is also quite effective for addressing the problem in this article.

Currently, a variety of optimal methods have been put for HAM. In order to obtain the better analytical solutions, Qian, Ren *et al.* (2012) put forward a new idea, which defined a kind of relative error of Δ_m and provided a valid way to select optimal auxiliary parameters. Subsequently, Liao (2012) defined the square residual function instead of residual function to reduce the errors. So soon, Gepreel and Nofal (2015) disposed of the nonlinear partial fractional differential equation via the optimal homotopy analysis method (OHAM). With the purpose of further improve the accuracy of the analysis solutions, Yuan and Alam (2016) applied with particle swarm optimization to diminish the exact square residual error in optimal HAM. As matters stand, these methods have been widely applied to engineering and physics problems.

In what follows, the paper introduces the optimal extended homotopy analysis method (OEHAM) in section 2. Then a classical example is used to verify the accuracy of the method in section 3 and section 4. Finally, the article ends up with a conclusion in section 5.

2. Basic approaches of the OEHAM

Consider the MDOF dynamical system as follows

$$M \ddot{q}(x) + G \dot{q}(x) + K q(x) = F(\dot{q}(x), q(x), x), \quad x \in \Omega. \quad (2)$$

where q is a n -dimensional unknown vector, a dot indicates the derivative with respect to x . M , G and K are $n \times n$ mass, damping and stiffness matrixes respectively. F is the vector function of \dot{q} , q and x , and Ω shows the solution interval. If $F(\dot{q}, q, x) \equiv 0$, then Eq. (2) is an autonomous dynamical system. If $F(\dot{q}, q, x) \neq 0$, a dynamical system likes Eq. (2) should be called as a non-autonomous system. From Eq. (2), we define a nonlinear differential operator as follows

$$N[u(r, x)] = M \frac{\partial^2 u(r, x)}{\partial x^2} + G \frac{\partial u(r, x)}{\partial x} + K u(r, x) - F\left(\frac{\partial u}{\partial x}, u, x\right) \quad (3)$$

where $u(r, x)$ is an unknown vector function, r and x are spatial and time variables, respectively.

In Eq. (3), the unknown vector functions of $u(r, x)$, $\partial u(r, x)/\partial x$ and $\partial^2 u(r, x)/\partial x^2$ are, respectively

$$u(r, x) = (x_1(x), \dots, x_n(x))^T, \quad (4)$$

$$\frac{\partial u(r, x)}{\partial x} = \left(\frac{dx_1}{dx}, \dots, \frac{dx_n}{dx} \right)^T, \quad (5)$$

and

$$\frac{\partial^2 u(r, x)}{\partial x^2} = \left(\frac{d^2 x_1}{dx^2}, \dots, \frac{d^2 x_n}{dx^2} \right)^T. \quad (6)$$

On the basis of the underlying principle of the EHAM, we construct the so-called zero-order deformation equation as follows

$$(1-p)\{L[\Phi(r, x; p) - u_0(r, x)]\} = p \hbar_1 H_1(x) N[\Phi(r, x; p)] + \hbar_2 H_2(x) \Pi[\Phi(r, x; p)], \quad (7)$$

Where $p \in [0, 1]$ is an embedding parameter, $u_0(r, x)$ is the solution of initial guess, L is an auxiliary linear operator, \hbar_i and $H_i(x)$ are the convergence-control parameters and the functions, respectively ($i=1, 2$).

While the operator $\Pi[\Phi(r, x; p)]$ has the following character

$$\Pi[\Phi(r, x; 0)] = \Pi[\Phi(r, x; 1)] = 0. \quad (8)$$

Clearly, for the zero-order deformation Eq. (7), we have the solution $\Phi(r, x; 0) = u_0(r, x)$, when $p=0$, and $\Phi(r, x; 1) = u(r, x)$, when $p=1$. Thus, as p raises from 0 to 1, the solution $\Phi(r, x; p)$ changes from the initial guess solution $u_0(r, x)$ to the exact solution $u(r, x)$.

Define

$$u_m(r, x) = \frac{1}{m!} \left. \frac{\partial^m \Phi(r, x; p)}{\partial p^m} \right|_{p=0}, \quad (9)$$

and expanding $\Phi(r, x; p)$ with the Taylor series expansion about the embedding parameter p in the sight of the theorem of vector-valued function, we obtain

$$\Phi(r, x; p) = u_0(r, x) + \sum_{m=1}^{+\infty} u_m(r, x) p^m. \quad (10)$$

If the auxiliary linear operator, initial guess solution, convergence-control parameters \hbar_1 , \hbar_2 and auxiliary functions $H_1(x)$, $H_2(x)$ are becomingly selected, the series Eq. (9) converges at $p=1$, so we obtain the series solution as follow

$$u(r, x) = u_0(r, x) + \sum_{m=1}^{+\infty} u_m(r, x). \quad (11)$$

For the purpose of simplicity, the vector of \mathbf{u}_m is defined as

$$\mathbf{u}_m = \{u_0(r, x), u_1(r, x), \dots, u_m(r, x)\}. \quad (12)$$

Differentiating the zero-order deformation Eq. (7) m times with respect to p , then dividing the equation by $m!$ and setting $p=0$, we can get

$$L[u_m(r, x) - \chi_m u_{m-1}(r, x)] = \hbar_1 H_1(x) R_m(\mathbf{u}_{m-1}, r, x) + \hbar_2 H_2(x) \Delta_m(r, x), \quad (13)$$

where

$$\chi_m = \begin{cases} 0, & m \leq 1 \\ 1, & m > 1 \end{cases}, \quad (14)$$

and

$$R_m(\mathbf{u}_{m-1}, r, x) = \frac{1}{(m-1)!} \frac{\partial^{m-1} N(\Phi(r, x; p))}{\partial p^{m-1}} \Big|_{p=0}, \quad (15)$$

$$\Delta_m(r, x) = \frac{1}{m!} \frac{\partial^m \Pi(\Phi(r, x; p))}{\partial p^m} \Big|_{p=0}. \quad (16)$$

The m -order deformation Eq. (13) is a linear equation, which can be lightly solved by the symbolic software such as Maple and Mathematica.

In order to value the precision of the m -order approximation of $u(r, x)$, the squared residual for the Eq. (2) is defined as follow

$$E_m = \int_{\Omega} \left| N \left[\sum_{m=0}^{+\infty} u_{1,m}(r, x) \right] \right|^2 dx. \quad (17)$$

If E_m is enough small, we can say that the m -order approximation of $u(r, x)$ is more precision. Given the initial guess solution $u_0(r, x)$, auxiliary functions $H_i(x)$ ($i=1,2$), and linear operator L , the squared residual E_m is dependent on the convergence-control parameters \hbar_i ($i=1,2$). Hence, unlike other analytic methods, the OEHAM presents an artful method to dominate the convergence of series solutions. The proof of the convergence of OEHAM solutions for the MDOF nonlinear dynamical system (2) is presented in Appendix A.

3. Application of the OEHAM

In this section, we apply the OEHAM to analyze the following damped Duffing resonator driven by a van der Pol oscillator

$$\begin{cases} \ddot{x}_1 + \varepsilon_1 \dot{x}_1 + \Omega_1^2 x_1 + k_1 x_1^3 - k_c(x_2 - x_1) = 0 \\ \ddot{x}_2 + \varepsilon_2(x_2^2 - 1)\dot{x}_2 + \Omega_2^2 x_2 - k_c(x_1 - x_2) = 0 \end{cases}. \quad (18)$$

Introducing $\tau = \omega t$ and substituting $x_1(t) = u_1(\tau)$, $x_2(t) = u_2(\tau)$ into Eq. (18), yield

$$\begin{cases} \omega^2 u_1''(\tau) + \omega \varepsilon_1 u_1'(\tau) + \Omega_1^2 u_1(\tau) + k_1 u_1^3(\tau) - k_c[u_2(\tau) - u_1(\tau)] = 0 \\ \omega^2 u_2''(\tau) + \omega \varepsilon_2 [u_2^2(\tau) - 1] u_2'(\tau) + \Omega_2^2 u_2(\tau) - k_c[u_1(\tau) - u_2(\tau)] = 0 \end{cases} \quad (19)$$

with the initial conditions

$$u_1(0) = a, \quad u_1'(0) = b, \quad u_2(0) = c, \quad u_2'(0) = 0, \quad (20)$$

where (') shows the derivative with respect to τ .

Consequently, the solutions in Eq. (19) can be expressed by a set of base functions $\{\cos(k\tau), \sin(k\tau) | k=0,1,2,\dots\}$, as follows

$$x_i(\tau) = \sum_{k=0}^{+\infty} (a_{i,k} \cos k\tau + b_{i,k} \sin k\tau), \quad (i=1, 2). \quad (21)$$

With regard to the initial approximation, we suppose

$$u_{1,0}(\tau) = a_0 \cos \tau + b_0 \sin \tau, \quad u_{2,0}(\tau) = c_0 \cos \tau, \quad (22)$$

and the linear operator is

$$L \begin{pmatrix} \Phi_1(\tau, q) \\ \Phi_2(\tau, q) \end{pmatrix} = \omega_0^2 \begin{pmatrix} \frac{\partial^2 \Phi_1(\tau, q)}{\partial \tau^2} + \Phi_1(\tau, q) \\ \frac{\partial^2 \Phi_2(\tau, q)}{\partial \tau^2} + \Phi_2(\tau, q) \end{pmatrix}, \quad (23)$$

with the character

$$L \begin{pmatrix} C_1 \sin \tau + C_2 \cos \tau \\ C_3 \sin \tau + C_4 \cos \tau \end{pmatrix} = 0. \quad (24)$$

According Eq. (19), we define the nonlinear operator as follows

$$N \begin{pmatrix} \Phi_1(\tau, q) \\ \Phi_2(\tau, q) \end{pmatrix} = \begin{pmatrix} \Omega^2(q) \frac{\partial^2 \Phi_1(\tau, q)}{\partial \tau^2} + \Omega(q) \varepsilon_1 \frac{\partial \Phi_1(\tau, q)}{\partial \tau} + \Omega_1^2 \Phi_1(\tau, q) + k_1 \Phi_1^3(\tau, q) - k_c [\Phi_2(\tau, q) - \Phi_1(\tau, q)] \\ \Omega^2(q) \frac{\partial^2 \Phi_2(\tau, q)}{\partial \tau^2} + \Omega(q) \varepsilon_2 \frac{\partial \Phi_2(\tau, q)}{\partial \tau} [\Phi_2^2(\tau, q) - 1] + \Omega_2^2 \Phi_2(\tau, q) - k_c [\Phi_1(\tau, q) - \Phi_2(\tau, q)] \end{pmatrix}. \quad (25)$$

The zero-order deformation equation can be written as follows

$$\begin{aligned} (1-q)L \begin{pmatrix} \Phi_1(\tau, q) - u_{1,0}(\tau) \\ \Phi_2(\tau, q) - u_{2,0}(\tau) \end{pmatrix} &= q \hbar_1 N \begin{pmatrix} \Phi_1(\tau, q) \\ \Phi_2(\tau, q) \end{pmatrix} \\ &+ (1-q) \hbar_2 \begin{pmatrix} A(q) \cos \tau + B(q) \sin \tau \\ C(q) \cos \tau \end{pmatrix} \\ &+ \begin{pmatrix} (\Omega^2(q) - \omega_0^2) (\cos \tau + \sin \tau) \\ (\Omega^2(q) - \omega_0^2) \sin \tau \end{pmatrix}, \end{aligned} \quad (26)$$

where

$$A(q) = \sum_{i=1}^{\infty} a_i q^i, \quad B(q) = \sum_{i=1}^{\infty} b_i q^i, \quad C(q) = \sum_{i=1}^{\infty} c_i q^i, \quad (27)$$

with the initial conditions

$$\Phi_1(0, q) = a_0 + A(q), \quad \frac{\partial \Phi_1(\tau, q)}{\partial \tau} \Big|_{\tau=0} = b_0 + B(q), \quad (28a)$$

$$\Phi_2(0, q) = c_0 + C(q), \quad \frac{\partial \Phi_2(\tau, q)}{\partial \tau} \Big|_{\tau=0} = 0. \quad (28b)$$

With regard to $q=0$, the solutions of Eqs. (26)-(28) are

$$\begin{pmatrix} \Phi_1(\tau, 0) \\ \Phi_2(\tau, 0) \end{pmatrix} = \begin{pmatrix} u_{1,0}(\tau) \\ u_{2,0}(\tau) \end{pmatrix}, \quad \Omega(0) = \omega_0. \quad (29)$$

However, for $q=1$, the zero-order deformation Eqs. (26)-(28) are equivalent to the primitive Eqs. (19)-(20), as follows

$$\begin{pmatrix} \Phi_1(\tau, 1) \\ \Phi_2(\tau, 1) \end{pmatrix} = \begin{pmatrix} u_1(\tau) \\ u_2(\tau) \end{pmatrix}, \quad \Omega(1) = \omega. \quad (30)$$

When the embedding parameter q increases from 0 to 1, $\Phi_i(\tau, q)$ changes from the initial guess $x_{i,0}(\tau)$ to the unknown solution $x_i(\tau)$ ($i=1,2$). Similarly, $\Omega(q)$ changes from the initial guess frequency ω_0 to the physical frequency ω .

Using the Taylor series expansion and Eq. (29), we can obtain

$$\Phi_1(\tau, q) = u_{1,0}(\tau) + \sum_{m=1}^{+\infty} u_{1,m}(\tau) q^m, \quad (31a)$$

$$\Phi_2(\tau, q) = u_{2,0}(\tau) + \sum_{m=1}^{+\infty} u_{2,m}(\tau) q^m, \quad (31b)$$

$$\Omega(q) = \omega_0 + \sum_{m=1}^{+\infty} \omega_m q^m, \quad (31c)$$

where

$$u_{1,m}(\tau) = \frac{1}{m!} \left. \frac{\partial^m \Phi_1(\tau, q)}{\partial q^m} \right|_{q=0}, \quad (32a)$$

$$u_{2,m}(\tau) = \frac{1}{m!} \left. \frac{\partial^m \Phi_2(\tau, q)}{\partial q^m} \right|_{q=0}, \quad (32b)$$

$$\omega_m = \frac{1}{m!} \left. \frac{\partial^m \Omega(q)}{\partial q^m} \right|_{q=0}. \quad (32c)$$

Selecting appropriate \hbar_1 and \hbar_2 , then the power series solutions in Eq. (31) converge at $q=1$. From Eqs. (29)-(30), we know that the series solutions are given by

$$u_1(\tau) = u_{1,0}(\tau) + \sum_{m=1}^{+\infty} u_{1,m}(\tau), \quad (33a)$$

$$u_2(\tau) = u_{2,0}(\tau) + \sum_{m=1}^{+\infty} u_{2,m}(\tau), \quad (33b)$$

$$\omega = \omega_0 + \sum_{m=1}^{+\infty} \omega_m. \quad (33c)$$

For the goal of simplicity, we define the vectors as

$$\mathbf{u}_n = \left\{ \begin{pmatrix} u_{1,0}(\tau) \\ u_{2,0}(\tau) \end{pmatrix}, \begin{pmatrix} u_{1,1}(\tau) \\ u_{2,1}(\tau) \end{pmatrix}, \dots, \begin{pmatrix} u_{1,n}(\tau) \\ u_{2,n}(\tau) \end{pmatrix} \right\},$$

$$\boldsymbol{\omega}_n = \{ \omega_0, \omega_1, \dots, \omega_n \} \quad (34)$$

Differentiating the zero-order deformation Eq. (26) m times with respect to p , then the resulting equation is divided by $m!$. And setting $p=0$, the m -order deformation equation is expressed as follows

$$\begin{aligned} & L \begin{pmatrix} u_{1,m}(\tau) - \chi_m u_{1,m-1}(\tau) \\ u_{2,m}(\tau) - \chi_m u_{2,m-1}(\tau) \end{pmatrix} \\ &= \hbar_1 \begin{pmatrix} R_{1,m}(\mathbf{u}_{m-1}, \boldsymbol{\omega}_{m-1}) \\ R_{2,m}(\mathbf{u}_{m-1}, \boldsymbol{\omega}_{m-1}) \end{pmatrix} + \hbar_2 \begin{pmatrix} S_{1,m}(\tau, \boldsymbol{\omega}_m) \\ S_{2,m}(\tau, \boldsymbol{\omega}_m) \end{pmatrix}, \end{aligned} \quad (35)$$

with the initial conditions

$$u_{1,m}(0) = a_m, \quad u'_{1,m}(0) = b_m, \quad (36a)$$

$$u_{2,m}(0) = c_m, \quad u'_{2,m}(0) = 0 \quad (m \geq 1), \quad (36b)$$

where

$$\begin{pmatrix} R_{1,m}(\mathbf{u}_{m-1}, \boldsymbol{\omega}_{m-1}) \\ R_{2,m}(\mathbf{u}_{m-1}, \boldsymbol{\omega}_{m-1}) \end{pmatrix} = \frac{1}{(m-1)!} \left. \frac{\partial^{m-1} N \begin{pmatrix} \Phi_1(\tau, q) \\ \Phi_2(\tau, q) \end{pmatrix}}{\partial q^{m-1}} \right|_{q=0}, \quad (37)$$

$$\begin{pmatrix} S_{1,m}(\tau, \boldsymbol{\omega}_m) \\ S_{2,m}(\tau, \boldsymbol{\omega}_m) \end{pmatrix}$$

$$= \begin{pmatrix} \left(\sum_{i=0}^m \omega_i \omega_{m-i} - \chi_m \sum_{i=0}^{m-1} \omega_i \omega_{m-1-i} \right) (\cos \tau + \sin \tau) \\ \left(\sum_{i=0}^m \omega_i \omega_{m-i} - \chi_m \sum_{i=0}^{m-1} \omega_i \omega_{m-1-i} \right) \sin \tau \\ + [Q_m(\boldsymbol{\delta}_m) - \chi_m Q_{m-1}(\boldsymbol{\delta}_{m-1})], \end{pmatrix} \quad (38)$$

and

$$Q_m(\boldsymbol{\delta}_m) = \begin{pmatrix} a_m \cos \tau + b_m \sin \tau \\ c_m \cos \tau \end{pmatrix}. \quad (39)$$

According to the rule of solution expression, the solutions that we obtain from Eq. (34) should not contain secular terms $\tau \sin \tau$ and $\tau \cos \tau$, so the right hand side of Eq. (36) must not contain the terms $\sin \tau$ and $\cos \tau$. Consequently, we obtain four algebraic equations

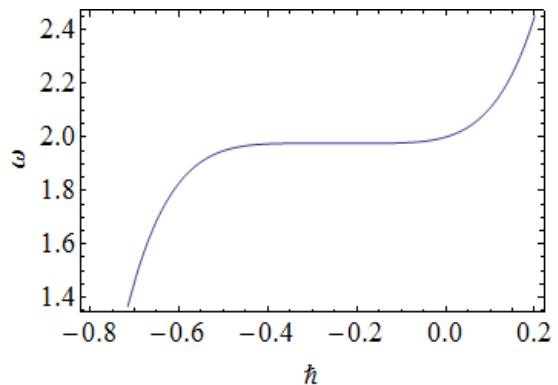


Fig. 1 The curve of $\omega - \hbar$

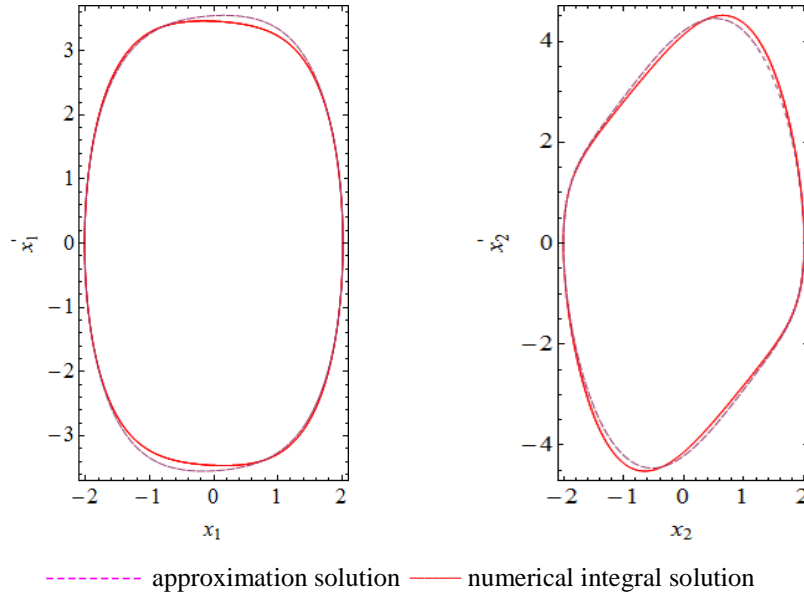


Fig. 2 Comparison the 4th-order phase diagram of HAM and Runge-Kutta method

$$\frac{1}{\pi} \int_0^{2\pi} [\hbar_1 R_{1,m}(\mathbf{u}_{m-1}, \boldsymbol{\omega}_{m-1}) + \hbar_2 S_{1,m}(\boldsymbol{\tau}, \boldsymbol{\omega}_m)] \cos \tau \, d\tau = 0 \quad (40a)$$

$$\frac{1}{\pi} \int_0^{2\pi} [\hbar_1 R_{1,m}(\mathbf{u}_{m-1}, \boldsymbol{\omega}_{m-1}) + \hbar_2 S_{1,m}(\boldsymbol{\tau}, \boldsymbol{\omega}_m)] \sin \tau \, d\tau = 0 \quad (40b)$$

$$\frac{1}{\pi} \int_0^{2\pi} [\hbar_1 R_{2,m}(\mathbf{u}_{m-1}, \boldsymbol{\omega}_{m-1}) + \hbar_2 S_{2,m}(\boldsymbol{\tau}, \boldsymbol{\omega}_m)] \cos \tau \, d\tau = 0 \quad (40c)$$

$$\frac{1}{\pi} \int_0^{2\pi} [\hbar_1 R_{2,m}(\mathbf{u}_{m-1}, \boldsymbol{\omega}_{m-1}) + \hbar_2 S_{2,m}(\boldsymbol{\tau}, \boldsymbol{\omega}_m)] \sin \tau \, d\tau = 0 \quad (40d)$$

With regard to Eqs. (35)-(40), we can obtain the solutions of ω_k , a_k , b_k , c_k ($k=0,1,2,\dots$). To measure whether the solutions $\begin{pmatrix} u_1(\tau) \\ u_2(\tau) \end{pmatrix}$ are sufficiently approximate, we can

use Mathematica to calculate the value of E_m . If the value diminishes to zero quickly, it indicates that the convergence control parameters \hbar_i ($i=1,2$) is optimal.

4. Numerical simulation and discussion

In this section, numerical experiment is used to verify the precision of the present method. From the previous description, two auxiliary nonzero parameters \hbar_1 and \hbar_2 are used to guarantee the convergence of the series solution. Obviously, if the range of the convergence control parameters is confirmed, accurate solutions of the researched problem will be obtained. By depicting the ω - \hbar_1 - \hbar_2 surface, we survey that solutions of ω is converged in a certain range. Therefore, the optimal \hbar_1 and \hbar_2 will be selected.

Firstly, we consider $\varepsilon_1=0$, $\varepsilon_2=0$, $\Omega_1=1$, $\Omega_2=2$, $k_1=1$, $k_c=1$ and the initial approximations of a , b , c , ω are $a_0=2$, $b_0=0$, $c_0=2$, $\omega_0=2$. In addition, we note that there exists two auxiliary parameters \hbar_1 and \hbar_2 , which are used to ensure the convergence of series solutions.

When $\hbar_2=0$, we use the classical HAM, then the fifth-order approximation of ω - \hbar_1 curve is given in Fig. 1. Obviously, we observe that the series solution of ω converge at $-0.5 < \hbar_1 < 0$, so we select $\hbar_1 = -0.1$ as well. Then the phase curves and the time history responses of the forth-order approximation are portrayed readily in Figs. 2(a)-(b) and Figs. 3(a)-(d), respectively.

Usually in this case, we acquire the numerical integration solution via the standard Runge-Kutta method, and the initial conditions of the numerical integration are based on $x_1(0)=2.000043$, $x_1'(0)=0.2563770$, $x_2(0)=2.000729$, $x_2'(0)=0$. In addition, the analytical approximation solutions for $x_1(t)$, $x_2(t)$ and ω of the second-order are expressed by

$$\begin{aligned} x_1(t) = & 1.95930054 \cos \omega t \\ & + 0.04042969 \cos 3\omega t + 0.00031250 \cos 5\omega t + \\ & 0.23762696 \sin \omega t \\ & + 0.00625000 \sin 3\omega t - 0.00156250 \sin 5\omega t, \end{aligned} \quad (41a)$$

$$\begin{aligned} x_2(t) = & 1.99562500 \cos \omega t \\ & + 0.00718750 \cos 3\omega t - 0.00208333 \cos 5\omega t + \\ & 0.24114257 \sin \omega t \\ & - 0.08038086 \sin 3\omega t + 0.01041667 \sin 5\omega t, \end{aligned} \quad (41b)$$

$$\omega = 1.98448254. \quad (41c)$$

From above pictures, it is clear that the current approximation solutions match the numerical integration solutions well.

However, in recently, a series of optimal HAM methods

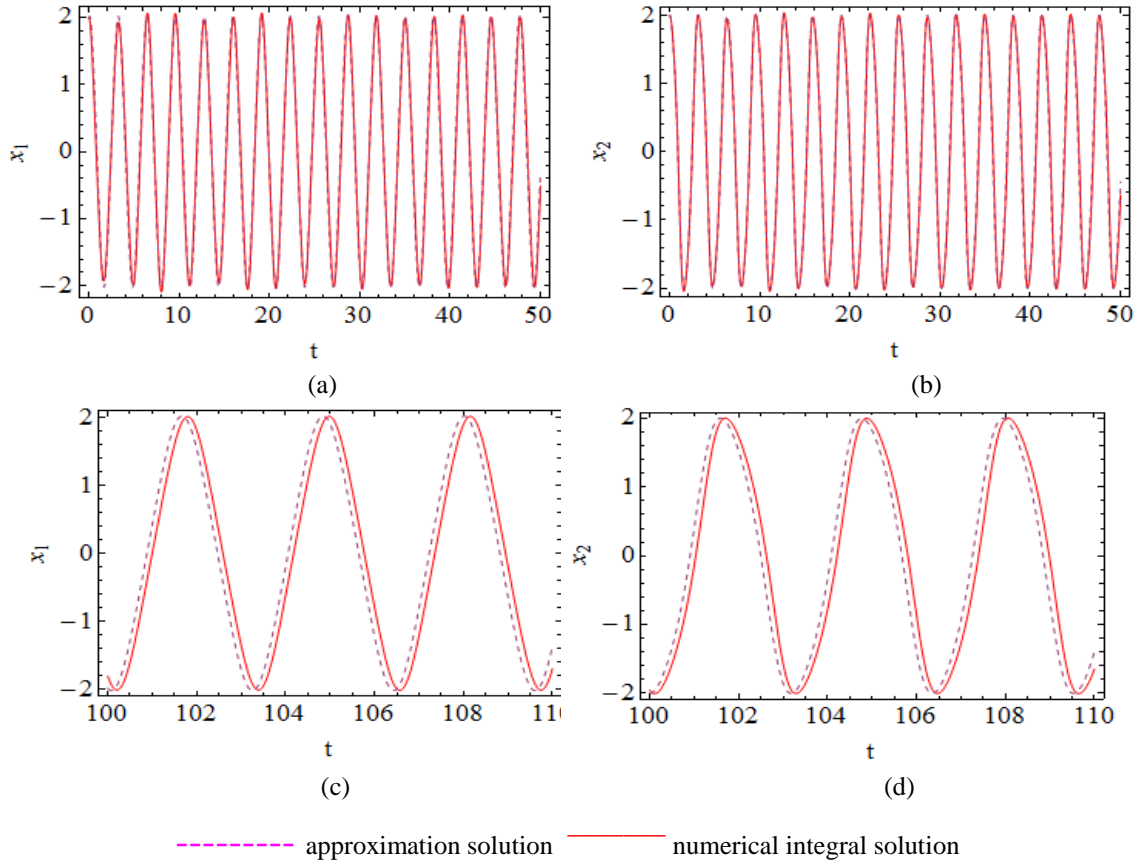


Fig. 3 Comparison the 4th-order time history diagram of HAM and Runge-Kutta method

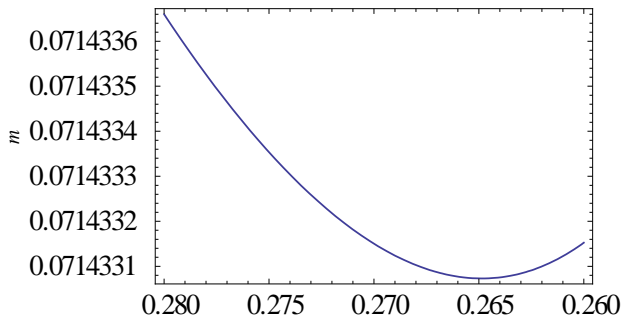


Fig. 4 The curve of $\Delta_m - \hbar$

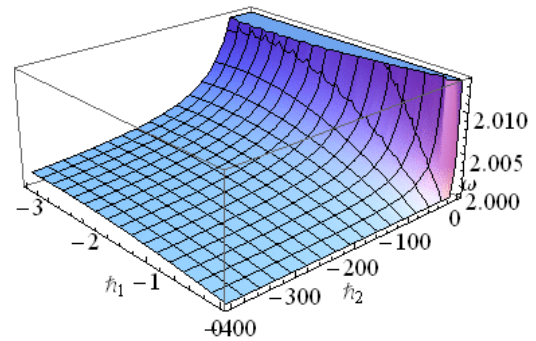


Fig. 5 The surface of $\omega - \hbar_1 - \hbar_2$

have been developed, which allow us to obtain faster convergent region of the analytical solutions. For the example in this article, we note that frequency and amplitudes of vibration are the most symbolic parameters in the analysis. Therefore, we can define the exact residual error of the m -order approximation as follows

$$\Delta_m = \frac{\sqrt{\left(\omega - \sum_{i=1}^m \omega_i\right)^2 + \left(a - \sum_{i=1}^m a_i\right)^2 + \left(c - \sum_{i=1}^m c_i\right)^2}}{20}, \quad (42)$$

where ω , a and c denote respectively the physical frequency and amplitude of $\begin{pmatrix} x_1(t) \\ x_2(t) \end{pmatrix}$ in Eq. (18). From Fig. 4 we observe that Δ_m decreases quickly to zero. Obvious, the convergence speed of the optimal homotopy series solutions

are faster than before in this area. In other words, by reducing the relative error, we can depict $\Delta_m - \hbar_1$ curve to acquire a better convergence control parameter, which can ensure the m -order series convergence faster in a large range. So the optimal \hbar_1 is obtained by the above approach. Obviously, by choosing $\hbar_1 = -0.265$, we can acquire more excellent solutions. However, the above situation is so peculiar that do not have strong stringency. So the second case ($\varepsilon_1 \neq 0$) was discussed as follows.

Secondly, we consider the case of $\varepsilon_1=0.025$, $\varepsilon_2=0.25$, $\Omega_1=1$, $\Omega_2=2$, $k_1=1$, $k_c=1$. In order to obtain a better solution, the EHAM ($\hbar_2 \neq 0$) was used to solve the problem. Similarly, showing the surface in Fig. 5 and selecting the effective domain of $\omega - \hbar_1 - \hbar_2$. Obviously, the series of ω

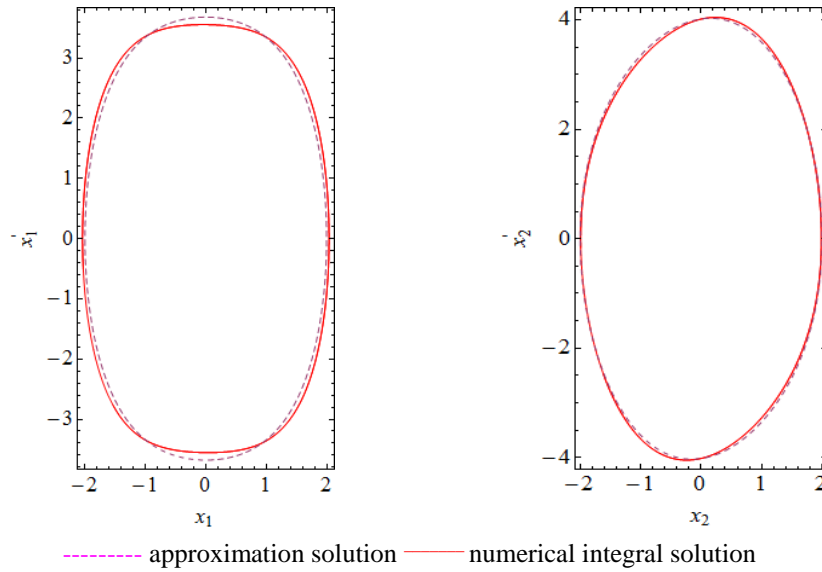


Fig. 6 Comparison the 2th-order phase diagram of HAM and Runge-Kutta method

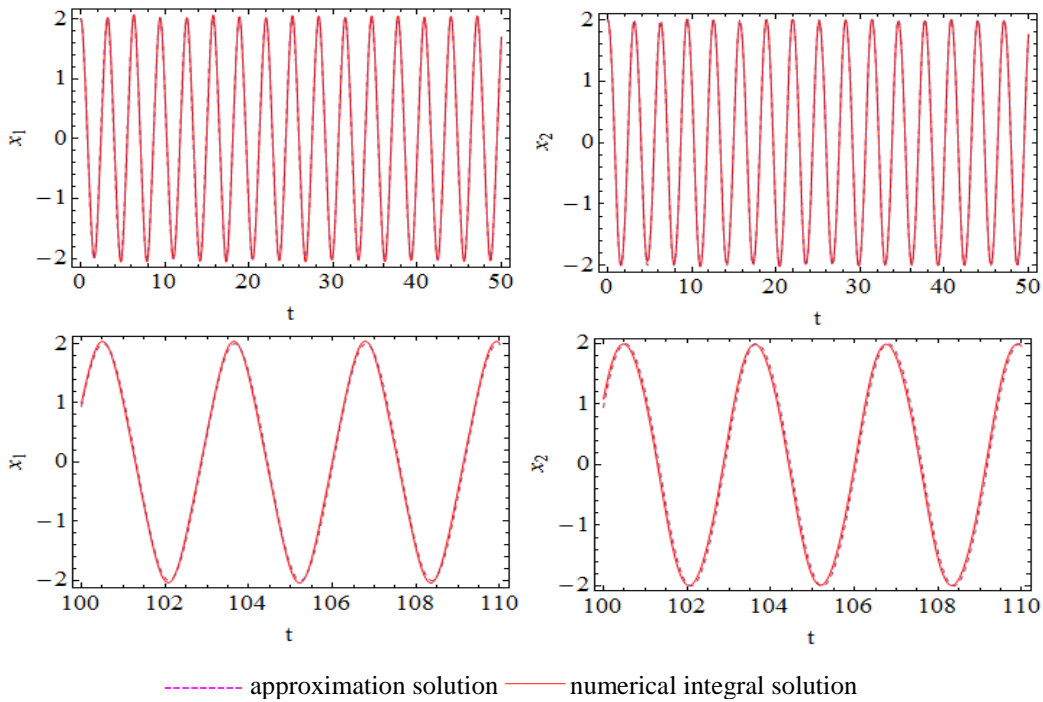


Fig. 7 Comparison the 2th-order time history diagram of HAM and Runge-Kutta method

convergence at $-0.5 < \hbar_1 < 0, -400 < \hbar_2 < -200$, so set $\hbar_1 = -0.1, \hbar_2 = -300, a_0=2, b_0=0, c_0=2, \omega_0=2$. The phase portraits and time history responses of the second-order approximation are portrayed respectively in Figs. 6(a)-(b) and Figs. 7(a)-(d). Apparently, we can conclude that the analytical approximation solutions and numerical solutions agree well with each other.

The numerical solutions are obtained by the standard Runge Kutta method, the addition conditions are based on $x_1(0)=1.99938, x_1'(0)=0.00064, x_2(0)=1.99999, x_2'(0)=0$. By the EHAM method, the analytical approximation solutions of the second-order are shown as follows

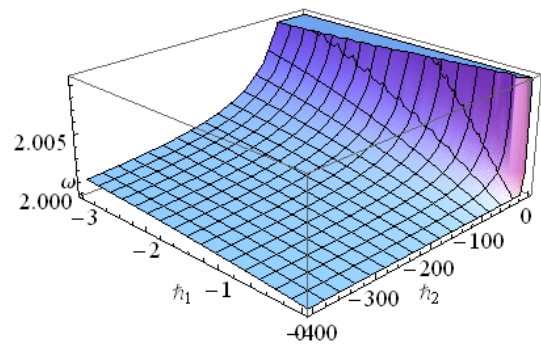


Fig. 8 The surface of $\omega - \hbar_1 - \hbar_2$

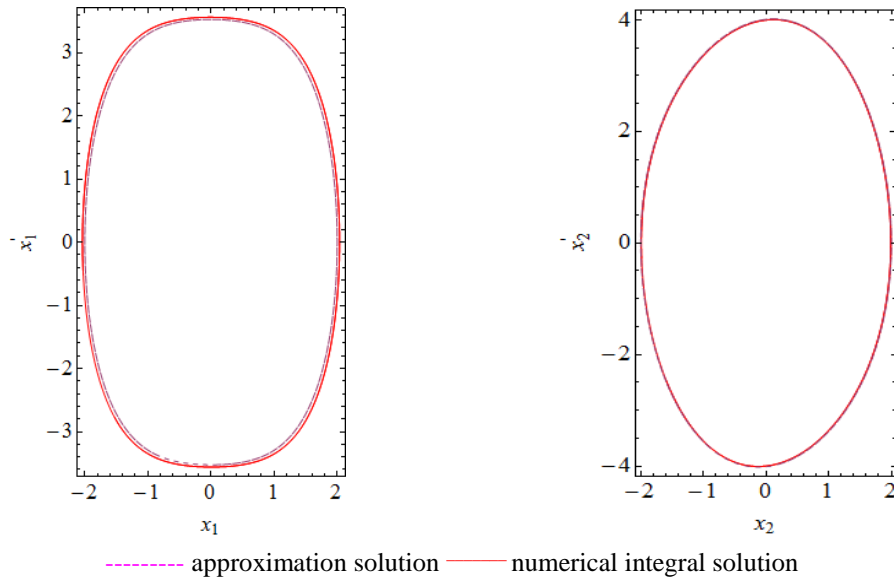


Fig. 9 Comparison the 2th-order phase diagram of HAM and Runge-Kutta method

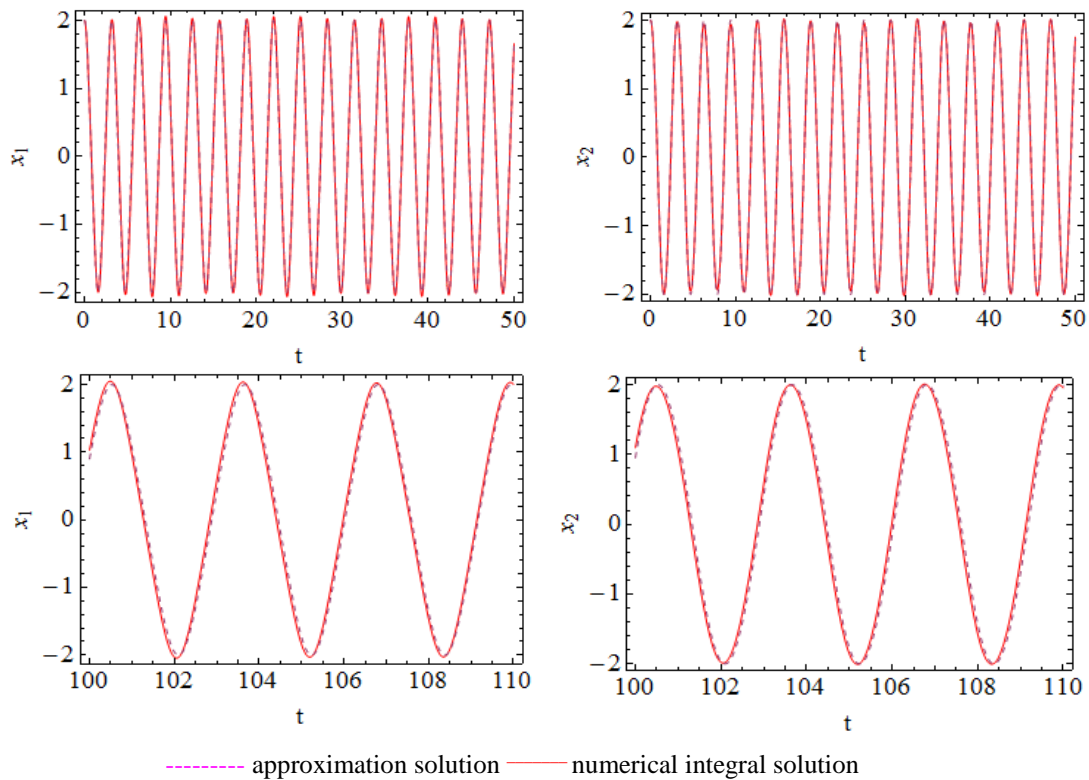


Fig. 10 Comparison the 2th-order time history diagram of HAM and Runge-Kutta method

$$\begin{aligned}
 x_1(t) &= 1.95876780\cos\omega t \\
 &+ 0.04030000\cos 3\omega t + 0.00031250\cos 5\omega t - \\
 &0.00107267\sin \omega t + 0.00014375\sin 3\omega t, \tag{43a}
 \end{aligned}$$

$$\begin{aligned}
 x_2(t) &= 2.00019593\cos\omega t \cdot \\
 &- 0.00007812\cos 3\omega t - 0.00013021\cos 5\omega t - \\
 &0.06047031\sin \omega t - 0.02015677\sin 3\omega t \tag{43b}
 \end{aligned}$$

$$\omega = 2.00016351. \tag{43c}$$

But there exist a little deviation when damping and coupling stiffness are powerful, which can be observed from Figs. 6-7.

Next, we will consider the weak situation. Set $\varepsilon_1=0.001$, $\varepsilon_2=0.125$, $\Omega_1=1$, $\Omega_2=2$, $k_1=1$, $k_c=0.5$ and regard $a_0=2$, $b_0=0$, $c_0=2$, $\omega_0=2$ as the initial approximation solution of a , b , c , ω . As before, the $\omega - \hbar_1 - \hbar_2$ curve is given in Fig. 8. Evidently, $-1 < \hbar_1 < 0$, $-500 < \hbar_2 < -300$, the series solution of ω is convergence. Thus, select $\hbar_1 = -0.2$, $\hbar_2 = -400$. In addition, the initial approximation solution

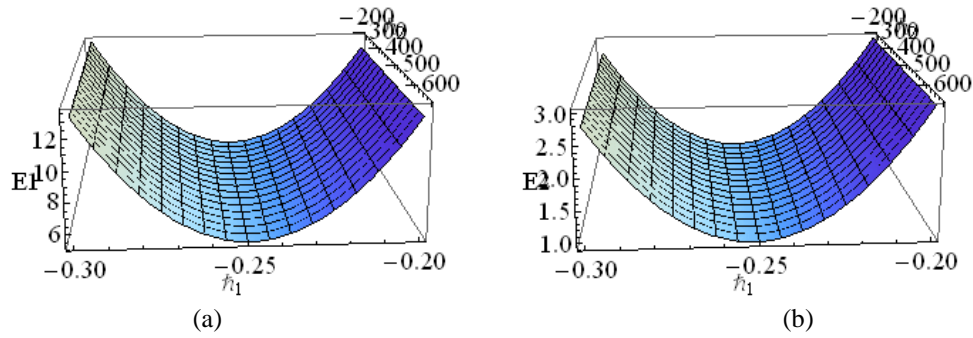


Fig. 11 The surface of $E_m - \hbar_1 - \hbar_2$

Table 1 Comparison with the exact frequencies ω_e and approximate frequencies ω_H , based on the non optimal \hbar_1 and \hbar_2

Ω_1	Ω_2	k_1	e_1	e_2	k_c	\hbar_1	\hbar_2	ω_e	ω_H	$\frac{ \omega_e - \omega_H }{\omega_e}$
1	4	1	0	1	1	-0.1	0	1.97581	1.97913	0.00168032
1	4	1	0.0025	0.25	1	-0.1	-300	1.98208	2.00047	0.00927813
1	4	1	0.001	0.125	0.5	-0.2	-400	1.98835	2.00032	0.00602007

Table 2 Comparison with the exact frequencies ω_e and approximate frequencies ω_H , based on the optimal \hbar_1 and \hbar_2

Ω_1	Ω_2	k_1	e_1	e_2	k_c	\hbar_1	\hbar_2	ω_e	ω_H	$\frac{ \omega_e - \omega_H }{\omega_e}$
1	4	1	0	1	1	-0.265	0	1.97581	1.97647	0.00033404
1	4	1	0.0025	0.25	1	-0.25	-500	1.98208	2.00046	0.00927309
1	4	1	0.001	0.125	0.5	-0.25	-500	1.98835	2.00024	0.00597983

of a, b, c, ω are $a_0=2, b_0=0, c_0=2, \omega_0=2$, and the phase diagram and the time history responses of the second-order approximation are plotted respectively in Figs. 9(a)-(b) and Figs. 10(a)-(d). We notice that the solutions of analytical approximation and numerical solutions fit well.

Similarly, we utilize the standard Runge-Kutta method to gain the numerical solution, with $x_1(0)=1.99959802, x_1'(0)=-0.00048111, x_2(0)=1.99998456, x_2'(0)=0$. More over, the analytical approximation solutions for $x_1(t), x_2(t)$ and ω of the second-order are expressed by

$$x_1(t) = 1.93774176 \cos \omega t + 0.06060625 \cos 3\omega t + 0.00125000 \cos 5\omega t - 0.00089316 \sin \omega t + 0.00013750 \sin 3\omega t, \quad (44a)$$

$$x_2(t) = 2.00050539 \cos \omega t - 0.00039061 \cos 3\omega t - 0.00013021 \cos 5\omega t + 0.04546992 \sin \omega t - 0.01515664 \sin 3\omega t, \quad (44b)$$

$$\omega = 2.00012264. \quad (44c)$$

From the above mentioned examples, we note that the EHAM is appropriate for the system of the damped Duffing resonator driven by a van der Pol oscillator with weak damping and coupling stiffness.

However, in recent years, a variety of optimal methods have been studied. In this article, we introduce an ingenious

mean to optimize the convergence domain of $\omega - \hbar_1 - \hbar_2$ surface. It is defined in Eq. (17), which denotes relative error of analytical approximation solutions. From Figs. 11(a)-(b), we can clearly observe that E_m reduce rapidly to zero in a certain area. It indicates that the series solution accelerate convergence in this region. Consequently, we can pick most appropriate \hbar_1 and \hbar_2 to obtain better analytical approximation solutions. It is clear that we can choose $\hbar_1 = -0.25, \hbar_2 = -500$.

To illustrate the correctness and accuracy of the optimal extend homotopy analysis method, the error estimation is presented as follows:

From Table 1 and Table 2, we note that the error of optimal approximate frequencies are small than the non optimal approximate frequencies. The exact frequency is computed using the numerical integration technique.

Now, we discuss the physical nature of the obtained solutions. Figs. 2 and 3 showed the phase curve and time-history response for the same set of initial conditions and governing parameters. In Fig. 2, curves for the approximate and numerical solutions are not closed to each other, but both solutions are very good as shown in Fig. 3. What is the reason why the difference between the approximate and numerical solutions in the phase curve is quite obvious, but not in the time-history response? Here, we would like to make a description: the time-history response just show

that, even if the time variable t progresses to a comparatively large domain, the results (i.e., phase curves and period solutions) obtained by the OEHAM will also be in good agreement with the numerical integration solution. In another word, the very good results in Fig.3 just guarantee the accuracy and validity of the results by Fig.2. If we get curves for the approximate and numerical solutions are closed to each other, but not good in time-history response or just good in short time, then we can say the approach is fail to solve the problem.

5. Conclusions

In this paper, the OEHAM is introduced to address a type of complex MDOF nonlinear systems. In particular, the damped Duffing resonator driven by a van der Pol oscillator is used to discuss as an example. To verify the correctness and accuracy of the method in the paper, some comparison between analytical approximation solutions and numerical integration solutions are studied. It is obvious that the analytical approximation solutions are in excellent agreement with the numerical integration solutions, under the condition of weak damping and coupling stiffness. Generally, it has a greater influence with the strong damping and coupling stiffness than weak damping and coupling stiffness, for the system of Duffing resonator driven by a van der Pol oscillator.

With the help of OEHAM, two cases are considered in this article, from which we can conclude that the OEHAM is more valid and available. On the one hand, it over comes the inconvenience of other analytical methods in dealing with complex MDOF nonlinear systems. On the other hand, it provides a valid way to choose auxiliary parameters.

Moreover, a variety of optimal methods have sprung up in recent years. For the example in the paper, we select squared residual to optimize the auxiliary parameters \hbar_1 and \hbar_2 . Obviously, the optimal analysis approximation solutions are coincidence with numerical solutions almost everywhere in convergence region. In brief, the above mentioned examples show that the actual method is appropriate for complex MDOF nonlinear systems. It is believed that the OEHAM can be further popularized for more complex nonlinear dynamic system.

Acknowledgements

The authors gratefully acknowledge the support of the National Natural Science Foundations of China (NNSFC) through grant Nos. 11202189 and 11572288, and the financial support of China Scholarship Council through grant No.201408330049. We are also grateful to the anonymous reviewers for their constructive comments and suggestions.

References

Bozyigit, B. and Yesilce, Y. (2016), "Dynamic stiffness approach

- and differential transformation for free vibration analysis of a moving Reddy-Bickford beam", *Struct. Eng. Mech.*, **58**(5), 847-868.
- Gepreel, K.A. and Nofal, T.A. (2015), "Optimal homotopy analysis method for nonlinear partial fractional differential equations", *Math. Sci.*, **9**(1), 47-55.
- Guo, Z.J., Leung, A.Y.T. and Yang, H.X. (2011a), "Oscillatory region and asymptotic solution of fractional van der Pol oscillator via residue harmonic balance technique", *Appl. Math. Model.*, **35**(35), 3918-3925.
- Guo, Z.J., Leung, A.Y.T. and Yang, H.X. (2011b), "Iterative homotopy harmonic balancing approach for conservative oscillator with strong odd-nonlinearity", *Appl. Math. Model.*, **35**(4), 1717-1728.
- Handam, A.H.H., Freihat, A.A. and Zurigat, M. (2015), "The multi-step homotopy analysis method for solving fractional-order model for HIV infection of CD4+T cells", *Proyecciones*, **34**(4), 307-322.
- Hoshyar, H.A., Ganji, D.D., Borran, A.R. and Falahati, M. (2015), "Flow behavior of unsteady incompressible Newtonian fluid flow between two parallel plates via homotopy analysis method", *Latin Am. J. Solid. Struct.*, **12**(10), 1859-1869.
- Leung, A.Y.T. and Guo, Z.J. (2010), "Residue harmonic balance for discontinuous nonlinear oscillator with fractional power restoring force", *Int. J. Nonlin. Sci. Numer. Simul.*, **11**(9), 705-723.
- Leung, A.Y.T. and Guo, Z.J. (2011), "Forward residue harmonic balance for autonomous and non-autonomous systems with fractional derivative damping", *Commun. Nonlin. Sci. Numer. Simul.*, **16**(4), 2169-2183.
- Liao, S.J. (1992), "The proposed homotopy analysis techniques for the solution of nonlinear problems", Ph.D. Dissertation, Shanghai Jiao Tong University, Shanghai.
- Liao, S.J. (2012), *Homotopy analysis method in nonlinear differential equations*, Higher Education Press, Beijing, China.
- Liu, L., Dowel, E.H. and Thomas, J.P. (2007), "A high dimensional harmonic balance approach for an aeroelastic airfoil with cubic restoring forces", *J. Fluid. Struct.*, **23**(3), 351-363.
- Lu, N.C., Cheng, Y.H., Li, X.G. and Jin, C. (2012), "Analytical solutions of dynamic mode I crack under the conditions of displacement boundary", *Nonlin. Dyn.*, **67**(3), 2197-2205.
- Lu, Z.H., Feng, Z.D. and Fang, C.L. (1991), "A new matrix perturbation method for analytical solution of complex modal eigenvalue problem of viscously damped linear vibration systems", *Appl. Math. Mech.*, **12**(8), 767-776.
- Odibat, Z.M. (2010), "A study on the convergence of homotopy analysis method", *Appl. Math. Comput.*, **217**(2), 782-789.
- Qian, Y.H. and Chen, S.M. (2010), "Accurate approximate analytical solution for multi-degree-of-freedom coupled van der Pol-Duffing oscillators by homotopy analysis method", *Commun. Nonlin. Sci. Numer. Simul.*, **15**(10), 3113-3130.
- Qian, Y.H., Ren, D.X., Lai, S.K. and Chen, S.M. (2012), "Analytical approximations to nonlinear vibration of an electrostatically actuated microbeam", *Commun. Nonlin. Sci. Numer. Simul.*, **17**(4), 1947-1955.
- Ray, S.S., Chaudhuri, K.S. and Betra, R.K. (2006), "Analytical approximate solution of nonlinear dynamic systems containing fractional derivatively by modified decomposition method", *Appl. Math. Comput.*, **182**(1), 544-552.
- Tasbozan, O., Esen, A. and Yagmurlu, N.M. (2012), "Approximate analytical solutions of fractional coupled mKdV equation by Homotopy analysis method", *Open J. Appl. Sci.*, **2**(3), 193-197.
- Vishal, K., Kumar, S. and Das, S. (2011), "Application of homotopy analysis method for fractional swift Hohenberg equation-revisited", *Appl. Mathem. Model.*, **36**(8), 3630-3637.
- Wei, X., Randrianandrasana, M.F., Ward, M. and Lowe, D. (2011),

“Nonlinear dynamics of a periodically driven duffing resonator coupled to a van der pol oscillator”, *Math. Prob. Eng.*, Article ID 248328, 16.

Xin, X.B., Kumar, S. and Kumar, D. (2015), “A modified homotopy analysis method for solution of fractional wave equations”, *Adv. Mech. Eng.*, **7**(12), 2015.

Yuan, L.G. and Alam, Z. (2016), “An optimal homotopy analysis method based on particle swarm optimization: Applization to fractional-order differential equation”, *J. Appl. Anal. Comput.*, **6**(1), 103-118.

Zhang, W., Qian, Y.H. and Lai, S.K. (2012), “Extended homotopy analysis method multi-degree-of-freedom non-autonomous nonlinear dynamical systems and its application”, *Acta Mechanica*, **223**(12), 2537-2548.

CC

Appendix A: Convergence theorem

In this section, the proof of the convergence of OEHAM solutions for the MDOF nonlinear dynamical system (2) is given as follows (Odibat 2010).

Theorem 1. If the Eq. (11) of the paper converges at $p=1$, and satisfies high-order deformation equation (13), (14), (15) and (16). Then Eq. (11) must be the solution of Eq. (2).

Proof. Due to the series $u(r, x) = u_0(r, x) + \sum_{m=1}^{+\infty} u_m(r, x)$ is convergent, let

$$Q(x) = \sum_{m=0}^{\infty} u_m(r, x) \text{ with } \lim_{m \rightarrow \infty} u_m(r, x) = 0. \quad (A1)$$

Then

$$\begin{aligned} & \sum_{m=1}^k [u_m(r, x) - \chi_m u_{m-1}(r, x)] \\ &= u_1(r, x) + u_2(r, x) - u_1(r, x) + u_3(r, x) \\ & \quad - u_2(r, x) + \dots + u_k(r, x) - u_{k-1}(r, x) \\ &= u_k(r, x). \end{aligned} \quad (A2)$$

So

$$\sum_{m=1}^{\infty} [u_m(r, x) - \chi_m u_{m-1}(r, x)] = \lim_{m \rightarrow \infty} u_m(r, x) = 0. \quad (A3)$$

However, operator L is linear, we can obtain that

$$\begin{aligned} & \sum_{m=1}^{\infty} L[u_m(r, x) - \chi_m u_{m-1}(r, x)] \\ &= L \sum_{m=1}^{\infty} [u_m(r, x) - \chi_m u_{m-1}(r, x)] = 0. \end{aligned} \quad (A4)$$

From Eq. (13) and Eq. (A4), we know that

$$\begin{aligned} & \sum_{m=1}^{\infty} L[u_m(r, x) - \chi_m u_{m-1}(r, x)] \\ &= \hbar_1 H_1(x) \sum_{m=1}^{\infty} R_m(u_{m-1}, r, x) + \hbar_2 H_2(x) \sum_{m=1}^{\infty} \Delta_m(r, x) = 0. \end{aligned} \quad (A5)$$

Because of $\hbar_1, \hbar_2, H_1, H_2$ can be chosen freely, the above equation could become a generalized equation as follows

$$\sigma_1(x) \sum_{m=1}^{\infty} R_m(u_{m-1}, r, x) + \sigma_2(x) \sum_{m=1}^{\infty} \Delta_m(r, x) = 0. \quad (A6)$$

Where $\sigma_i(t) \neq 0 (i=1,2)$.

From Eq. (15) and Eq. (16), we can obtain that

$$\begin{aligned} & \sigma_1(x) \sum_{m=1}^{\infty} \frac{1}{(m-1)!} \left. \frac{\partial^{m-1} N(\Phi(r, x; p))}{\partial p^{m-1}} \right|_{p=0} \\ & + \sigma_2(x) \sum_{m=1}^{\infty} \frac{1}{m!} \left. \frac{\partial^m \Pi(\Phi(r, x; p))}{\partial p^m} \right|_{p=0} = 0, \end{aligned} \quad (A7)$$

that is

$$\sigma_1(x) \sum_{m=0}^{\infty} \frac{1}{m!} \left. \frac{\partial^m N(\Phi(r, x; p))}{\partial p^m} \right|_{p=0}$$

$$+\sigma_2(x)\sum_{m=1}^{\infty}\frac{1}{m!}\frac{\partial^m\Pi(\Phi(r,x;p))}{\partial p^m}\Big|_{p=0}=0. \quad (\text{A8})$$

Let

$$\tau(r,x;p)=\sigma_1(x)N[\Phi(r,x;p)]+\sigma_2(x)\Pi[\Phi(r,x;p)], \quad (\text{A9})$$

and represents the residual error of Eq. (2). In order to prove Eq. (11) is the exact solution of Eq. (2), we need to prove $\tau(r,x;p)=0$.

From Eq. (A9), we can obtain the Maclaurin series of $\tau(r,x;p)$ on embedded variable p .

$$\begin{aligned} \tau(r,x;p) &= \sum_{m=0}^{\infty}\frac{\partial^m\tau(r,x;p)}{\partial p^m}\Big|_{p=0}\frac{p^m}{m!} \\ &= \sigma_1(x)\sum_{m=0}^{\infty}\frac{\partial^m(\Phi(r,x;p))}{\partial p^m}\Big|_{p=0}\frac{p^m}{m!} \\ &+ \sigma_2(x)\sum_{m=0}^{\infty}\frac{\partial^m\Pi(\Phi(r,x;p))}{\partial p^m}\Big|_{p=0}\frac{p^m}{m!} \\ &= \sigma_1(x)\sum_{m=0}^{\infty}\frac{\partial^m(\Phi(r,x;p))}{\partial p^m}\Big|_{p=0}\frac{p^m}{m!} \\ &+ \sigma_2(x)\sum_{m=1}^{\infty}\frac{\partial^m\Pi(\Phi(r,x;p))}{\partial p^m}\Big|_{p=0}\frac{p^m}{m!} \\ &\quad + \sigma_2(x)\Pi(\Phi(r,x;0)) \end{aligned} \quad (\text{A10})$$

So

$$\begin{aligned} \tau(r,x;1) &= \sigma_1(x)\sum_{m=0}^{\infty}\frac{\partial^m(\Phi(r,x;p))}{\partial p^m}\Big|_{p=0}\frac{1}{m!} \\ &+ \sigma_2(x)\sum_{m=1}^{\infty}\frac{\partial^m\Pi(\Phi(r,x;p))}{\partial p^m}\Big|_{p=0}\frac{1}{m!} \\ &\quad + \sigma_2(x)\Pi(\Phi(r,x;0)). \end{aligned} \quad (\text{A11})$$

From Eq. (8) and Eq. (A8), we know that

$$\tau(r,x;1)=\sum_{m=0}^{\infty}\frac{\partial^m\tau(r,x;p)}{\partial p^m}\Big|_{p=0}\frac{1}{m!}=0. \quad (\text{A12})$$

Thus, if Eq. (11) is convergent, it must be a solution of Eq. (2).